Journal of Power Sources 196 (2011) 10798–10805

Contents lists available at SciVerse ScienceDirect

Journal of Power Sources

journal homepage: www.elsevier.com/locate/jpowsour

Carbon-nanofiber counter electrodes for quasi-solid state dye-sensitized solar cells

Ganapathy Veerappan, Woosung Kwon, Shi-Woo Rhee*

System on Chip Chemical Process Research Center, Department of Chemical Engineering, Pohang University of Science and Technology (POSTECH), Pohang 790-784, Republic of Korea

ARTICLE INFO

Article history:
Received 14 June 2011
Received in revised form 29 August 2011
Accepted 1 September 2011
Available online 7 September 2011

Keywords:
Dye-sensitized solar cells
Carbon-nanofibers
Charge transfer resistance
Flexible counter electrode
Quasi-solid state electrolyte

ABSTRACT

Carbon-nanofibers (CNFs) with antler and herringbone structures are studied as a tri-iodide (I_3^-) reduction electrocatalyst in combination with the liquid electrolyte or an alternative stable quasi-solid state electrolyte. The catalytic properties of the counter electrode (CE) are characterized by cyclic voltammetry (CV) and electrochemical impedance spectroscopy (EIS). The doctor bladed low temperature CNFs-CE has faster I_3^- reduction rate and low charge transfer resistance (R_{CT}) of ~0.5 Ω cm^2 than platinum (Pt) (~2.3 Ω cm^2) due to the nanofiber stacking morphology. Its herringbone and antler structures with graphitic layers lead to defect rich edge planes and larger diameter of CNFs facilitate the electron transfer kinetics. The cells with CNF counter electrodes are showing promising energy conversion efficiency greater than 7.0% for the glass based devices and 5.0% for the flexible cells filled with the quasi-solid state electrolyte, which is similar to Pt performance. Application of CNFs-CE in flexible and quasi-solid state electrolyte increases the possibility of roll to roll process, low cost and stable dye-sensitized solar cells (DSCs).

1. Introduction

Low cost, non-vacuum and high energy conversion efficiency made dye-sensitized solar cells (DSCs) the most promising alternative to the conventional silicon-based solar cells [1–4]. Dye-sensitized solar cells main framework consists of two electrodes, namely photo electrode (PE) and a counter electrode (CE) and an electrolyte in between. Both electrodes were prepared on transparent conducting oxide (TCO) glass substrate. Platinum (Pt) has been used as a catalytic material for tri-iodide (I_3^-) reduction in DSCs due to its superior catalytic activity and good conductivity [5,6]. Though Pt has superior catalytic activity, it is a very expensive noble metal and scarce in the world. This necessitates the finding of an alternative catalytic material which is low-cost, low temperature processable, abundantly available in nature and at the same time, stable [7]. In recent years, some cost effective alternative materials such as carbon-nanotubes (CNTs), mesoporous carbon, graphite, carbon black, carbon composites, graphene and conducting polymers have been tried [8–18]. So far, the carbon films prepared by the doctor blading method exhibited good electrochemical property and conversion efficiency but all those reports included high temperature sintering and volatile liquid electrolytes [12,13]. Problems associated with the liquid electrolyte can be solved by using quasi-solid state electrolyte with good thermal stability [9,19,20].

Due to the high temperature process in CE, very few groups have reported the flexible DSC. Low temperature DSCs have been made on flexible polymer substrates such as polyethylene terephthalate (PET) or polyethylene naphthalate (PEN) coated with conductive indium doped tin oxide (ITO) films but most of the reports were mainly aimed for flexible photo electrode [21]. Very few reports on the low temperature and flexible CE are available and their device performances are not so good in comparison with the Pt cells [21–24]. Till now, not much attention has been paid to the flexible CE and the quasi-solid state electrolyte in DSCs.

In this research, attempts were made to replace conventional Pt with two different carbon-nanofibers (CNFs) as CE catalysts. Also attempts were made to replace volatile liquid electrolyte with the quasi-solid state electrolyte as a redox mediator on flexible ITO/PET substrates. Electrochemical analysis was used to scrutinize the catalytic property of the CNFs-CE which is known to have a large number of edge plane sites along the surface of the tube [25–29]. Under 1 sun illumination (AM 1.5), the cells assembled with CNF on flexible ITO/PET or CNF on fluorine doped tin oxide (FTO) glass will be evaluated both with the liquid and the quasi-solid state electrolyte.

2. Experimental

2.1. Preparation of electrodes and electrolyte

Carbon-nanofiber counter electrodes (CNFs-CE) were prepared as follows. Two different types of commercially available TCOs; F:

* Corresponding author. Tel.: +82 54 279 2265; fax: +82 54 279 8619.
E-mail address: srhee@postech.ac.kr (S.-W. Rhee).

0378-7753/$ – see front matter © 2011 Elsevier B.V. All rights reserved.
doi:10.1016/j.jpowsour.2011.09.004

SnO_2 (FTO) coated glass plates and In: SnO_2 coated flexible polymer sheets (ITO/PET) with sheet resistance of ($8\ \Omega\ \square^{-1}$) and ($15\ \Omega\ \square^{-1}$), respectively were used. 0.5 g of CNF powder (Carbon nano-material tech. co., Republic of Korea, average diameter of 200 nm) was finely ground with mortar and pestle and then mixed with 2 g of the binder solution composed of 0.64 g carboxy-methyl cellulose (CMC) sodium salt in 39.68 ml deionized water. The resultant homogeneous, viscous paste was deposited on the cleaned FTO glass or ITO/PET plastic substrates using doctor blading to obtain films of thickness about 12 μm. The resulting film was kept outside for 7 min to have good leveling and to reduce the surface irregularity. Subsequently, the dried electrodes were baked at 100 °C in a vacuum oven for 5 h. Traditional Pt-CE was prepared for comparison by depositing Pt precursor (Plastisol, Solaronix) on the FTO glass substrate followed by sintering at 400 °C for 5 min and Pt on ITO/PET flexible substrates was deposited with sputtering.

The photo anode consisting of ~12 μm thick nanocrystalline TiO_2 layer (Ti-Nanoxide HT/SP from Solaronix) was prepared on the FTO glass substrate by screen printing. Then 3 μm thick light scattering layer (Ti-Nanoxide R/SP from Solaronix) was prepared onto the already prepared nanocrystalline TiO_2 layer with the same method for light reflecting property. After drying the electrode at 120 °C for 7 min, it was sintered at 500 °C for 30 min [11]. Once cooled down to 80 °C the sintered electrodes were immediately immersed in the 0.3 mM solution of N719 dye in a mixture of acetonitrile/tert-butanol (volume ratio 1:1) for 24 h.

The organic liquid electrolyte used in this work composed of 0.5 M 1-butyl-3-methyl imidazolium iodide (BMII), 0.06 M Iodine (I_2) and 0.5 M 4-tertbutylpyridine (tBP) in a acetonitrile solvent. The quasi-solid state electrolyte was prepared separately. 40 wt.% of poly (lactic-co-glycolic acid) (PLGA) was mixed with the liquid electrolyte consisting of 0.5 M BMII, 0.1 M potassium iodide (KI), and 0.06 M I_2 and dissolved in 20 ml acetonitrile solvent. The mixture was stirred overnight at 50 °C under argon atmosphere to form a homogeneous and viscous amphiphilic polymer gel electrolyte (APGE). Prior to use, the routine additives, 0.5 M tBP and 0.1 M guanidinium thiocyanate were added to the APGE.

2.2. Device fabrication

The dye-sensitized TiO_2 photo electrodes were removed from the dye solution and rinsed in ethanol and dried using nitrogen air blow. Simultaneously the doctor bladed CNFs-CE was removed from baking and both electrodes were assembled using Surlyn spacer with the photo electrodes and CNF or Pt counter electrodes. The liquid and quasi-solid state electrolyte were filled in each cell. The liquid or homogeneous viscous gel electrolyte was introduced into the cell through one of the two holes drilled in CE and the holes were sealed using Surlyn and a thin cover glass. After sealing the cell, a motionless polymer gel electrolyte could be observed inside the cell.

2.3. Characterization and measurements

The morphology of the CNF powders and films were investigated using field emission scanning electron microscopy (FE-SEM, JEOL JSM-7401F), atomic force microscopy (AFM, Veeco Nanoscope V), Brunauer–Emmett–Teller (BET) and high resolution transmission electron microscopy (HR-TEM, Hitachi H7650). In order to check its electrocatalytic property, cyclic voltammetry (CV) and electrochemical impedance spectroscopy (EIS) were utilized. The CV experiments were performed at a scan rate of $50\ mV\ s^{-1}$ with the Reference 600 potentiostat (Gamry instruments) in a three electrode configuration, a working electrode with thermally deposited Pt or doctor bladed CNFs, Pt coil as a counter electrode and silver/silver chloride as a reference electrode in the acetonitrile solution containing 10 mM lithium iodide (LiI), 1 mM I_2, and 0.1 M lithium perchlorate ($LiClO_4$). The EIS measurements were performed on the symmetric cells to investigate the I_3^- reduction activity by calculating the charge transfer resistance (R_{CT}) at the CE/electrolyte interface. The EIS measurements were carried out in the dark at room temperature in the frequency range from 100 mHz to 100 kHz at 0 voltage. Electrochemical parameters were derived from the ac impedance spectra by fitting the high frequency region using "Zfit" impedance analysis software [11,23]. The photocurrent–voltage (*I–V*) properties of the DSCs were studied by using AM 1.5 simulated solar light irradiation, calibrated by the standard Si solar cell. The light source equipped with 300 W xenon lamp (Newport, USA) was used. The *I–V* curves were obtained by applying an external bias to the cell and the generated photocurrent was measured with a Keithley model 2400 digital source meter.

3. Results and discussion

3.1. Electrochemical properties of CNF counter electrode

The schematic diagram shown in Fig. 1 illustrates the conceptual diagram of the catalytic sites for I_3^- reduction in various CNFs. The structure of hollow CNT, herringbone carbon-nanofiber (CNF-100) and antler carbon-nanofiber (CNF-LSA) were shown in Fig. 1a–c, respectively. CNFs might be more favorable for the catalytic reaction due to their defect rich edges and fiber stacking morphology [25–29]. Fig. 2a shows the CVs for the iodide (I^-)/I_3^- reduction reaction with the CNFs and Pt electrode. Two pairs of redox peaks were obtained in the CV curves for the CNF electrode which shows that the CNFs have Pt-like electrocatalytic feature [14,30]. The peaks in the positive side is known as the oxidation peak (1) and the negative one is the reduction peak (2). The kinetic reaction at the heterogeneous interface of the CE and the electrolyte for DSC is represented as follows [10,11,30].

$$3I^- \rightarrow I_3^- + 2e^- \quad \text{(oxidation)} \tag{1}$$

$$I_3^- + 2e^- \rightarrow 3I^- \quad \text{(reduction)} \tag{2}$$

In the cathodic peak, the current density of Pt is slightly higher than the CNF electrode, but it has an insignificant effect on the catalytic performance. On the other hand, the anodic peaks of the CNFs show higher current density than Pt, which has a direct influence on the photovoltaic and catalytic performance [30]. This shows that the CNFs can be a promising electrocatalytic material for DSCs. The electrocatalytic behavior of the CNFs is from the high surface area and stacking morphology. CNF-LSA shows higher current density than Pt and CNF-100, which is from the more open structure and defect rich edge planes of CNF-LSA (antler structure) compared to CNF-100 (herringbone structure) [25–29]. In their electrochemical studies of several carbon material, Compton et al. [26–28] found that bamboo, herringbone and antler shaped carbon-nanofibers exhibited a higher percentage of graphitic layers with a large number of edge-plane sites at the surface of the tube. These structures showed better electrochemical activity than the smooth, more basal plane-like structure [25–29]. The Nyquist plot of the symmetric cells made with CNFs and Pt can be analyzed from Fig. 2b. The semicircle observed in the low frequency region (right) is from the Nernst diffusion impedance in the redox electrolyte [31–34], whereas the high frequency semicircle (left) gives R_{CT}, an index of the catalytic property of the CNFs or Pt CE. R_{CT} is estimated from the real component of the impedance obtained by fitting with an equivalent circuit as shown in the inset of Fig. 2b [32,33]. In the equivalent circuit, one more diffusion (Z_W) term is included which originates from the charge transport inside the porous layer. Also its electrical conductivity is lower than Pt. The R_{CT} of the doctor bladed CNF electrode were found to be 0.5 and $0.6\ \Omega\ cm^2$ for

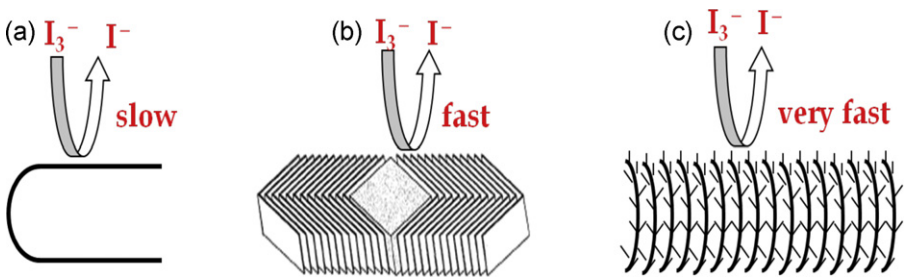

Fig. 1. Schematic diagram representing I_3^- reduction and oxidation on different fiber surfaces (a) Hollow CNFs (ordinary structure) (b) CNF-100 (herringbone structure) and (c) CNF-LSA (antler structure).

CNF-LSA and CNF-100, respectively, which were about half of the R_{CT} of thermally deposited Pt electrodes (1.2 Ω cm^2). The R_{CT} value clearly indicates that the catalytic property obtained with the CNF electrodes are better than Pt. The data from EIS analysis is consistent with the observation from the CV analysis shown in Fig. 2a.

Although the CNF electrodes show lower R_{CT}, they have high internal series resistance (R_S) (the starting point of the left circle: R_S) because CNF has higher resistance than Pt. Also the semicircle on the right hand side is larger for CNF because there is an additional diffusion resistance inside the pores of the carbon layer. The total internal series resistance of the cell (end of the right hand side circle on *x*-axis) is larger for CNF than conventional Pt counter electrode, which may affect the device performance parameters [12,35,36]. The optimization of carbon layer thickness is thus needed.

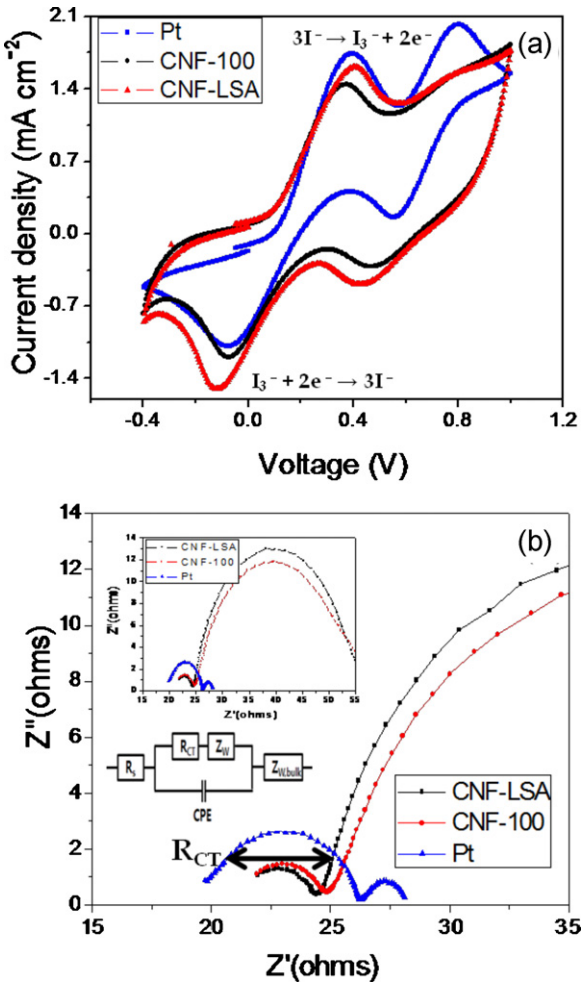

Fig. 2. Electrochemical characterization of CNFs and Pt using cyclic voltammograms and electrochemical impedance spectroscopy, (a) cyclic voltammograms obtained at a scan rate of 50 mV s^{-1} for the reduction of I^-/I_3^- on the CNFs and Pt electrodes, and (b) Nyquist plots of the symmetric cells with CNFs and Pt electrodes. Inset shows high and low frequency region and electrical circuit used to obtain the electrochemical parameters for CNFs.

3.2. Surface and structure morphology

To gain insight into the catalytic ability of the CNF CE, investigations on the surface configuration and morphology of the CNF electrodes were studied using FE-SEM, AFM, HR-TEM and BET analysis. The SEM surface morphology of the doctor bladed CNFs on a FTO glass substrate were presented in Fig. 3. The CNF films formed on the FTO substrates (Fig. 3a and c) are uniform with small aggregates and uneven size in the diameter of each fiber. During the paste preparation, the long CNFs (>20 μm) were broken into a few micron pieces but it did not affect the photovoltaic performance. In addition, AFM and SEM micrographs in Figs. 3 and 4 show very rough surface for both CNFs. AFM analysis showed the uniform distribution of fibers with larger surface area for both CNFs and Pt is composed of island like structure with smooth surface. The roughness of the film (root mean square) calculated from AFM measurements was 236 nm and 240 nm for CNF-LSA and CNF-100, respectively. Roughness of the film was also clearly seen in the FE-SEM surface analysis. The CNFs are mainly consisted of randomly oriented porous fiber network with high surface area and large fiber diameter, which is beneficial for the catalytic activity and the diffusion of a few angstrom I_3^- ions [10]. In fact, catalytic materials with the high surface area might have higher electrochemical property for I_3^- reduction rather than the small island like Pt structure [14,37]. Fig. 3b and 3d showed the magnified image of the CNFs with the herringbone and antler structure with a few microns in length.

The HR-TEM images in Fig. 5 shows highly disordered walls in CNF-100 and CNF-LSA with an average diameter of ≤200 nm, while Fig. 5a and 5b clearly show the herringbone (CNF-100) and antler structure at the edges (CNF-LSA), respectively. Since iron or other residual metal catalysts may react with the redox electrolyte used in the DSC, it may cause stability issues in the device. From the elemental mapping analysis (Fig. 5c–e) with energy dispersive X-ray spectroscopy(EDX) in scanning transmission electron microscopy (STEM), it was confirmed that the CNFs mainly composed of carbon and the amount of metal catalysts used for CNFs synthesis such as nickel or iron was below the detection limit. CNF-100 mainly composed of graphitic layers terminated at the surface and a large number of transverse walls with periodically closed compartments, which results in rougher and defected edge planes at the fiber surface. In the CNF-LSA, the walls are made of terminated graphitic surface similar to CNF-100. The transverse walls in CNF-LSA have open structure similar to the antler in a deer, which produces a highly catalytic region.

The nitrogen adsorption–desorption isotherms were measured and it showed type IV isotherm H2 hysteresis loops according to

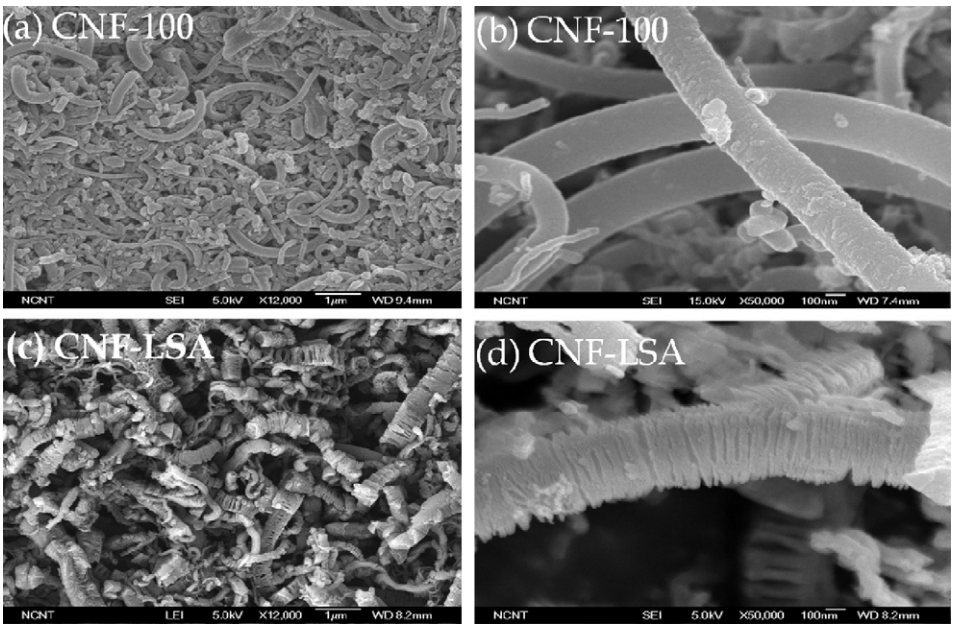

Fig. 3. FE-SEM surface morphology of the CNF powders and films deposited on FTO glass substrate (a) CNF-100 film, (b) magnified image of CNF-100 powder, (c) CNF-LSA film and (d) magnified image of CNF-LSA powder.

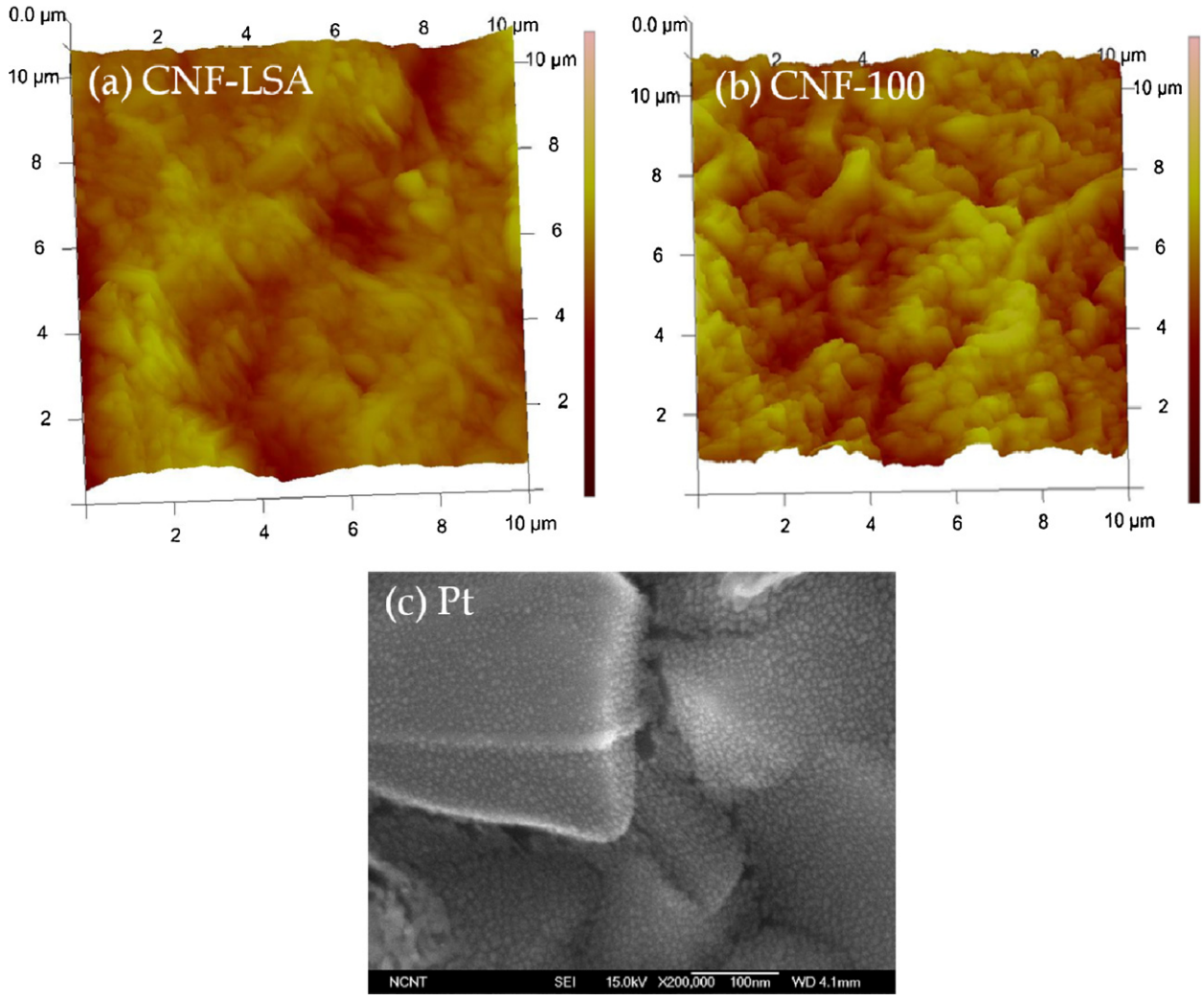

Fig. 4. AFM and SEM surface images for (a) CNF-LSA, (b) CNF-100 and (c) Pt.

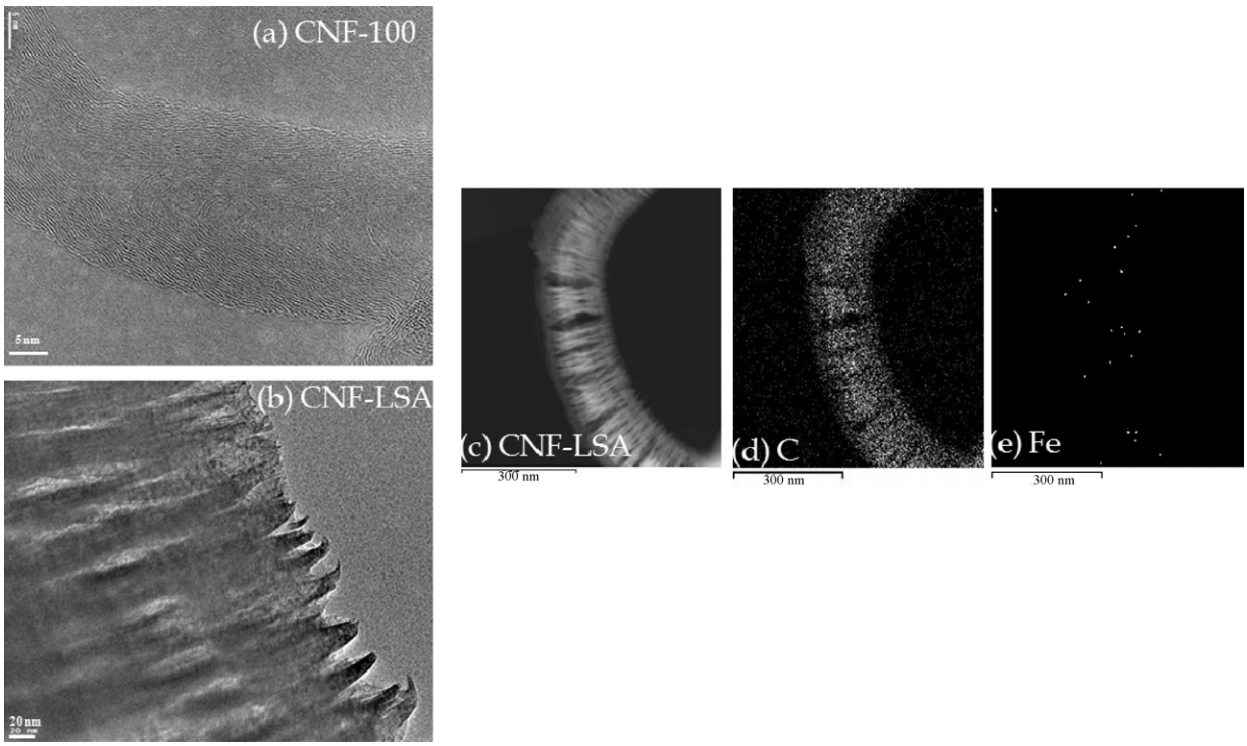

Fig. 5. HR-TEM images for herringbone and antler structure of (a) CNF-100, and (b) CNF-LSA. TEM image and EDX elemental mapping obtained with STEM, (c) CNF-LSA, (d) carbon and (e) iron catalyst.

IUPAC nomenclature. The BET surface areas were calculated to be about 153 and 116 $m^2\,g^{-1}$ for CNF-100 and CNF-LSA, respectively. Pore size distribution was not able to calculate due to the randomly oriented pores. With the fibrous morphology, porous structures were formed and it was also seen in the SEM and AFM images discussed above. The doctor-bladed film contains three-dimensional continuous macroporous/mesoporous network with several tens to several hundred nanometer sized pores with efficient transport pathways to I^-/I_3^- ions.

3.3. Photovoltaic performance of DSCs with CNF counter electrode (CE)

3.3.1. CNF counter electrode on FTO glass with liquid electrolyte

Fig. 6 shows the *I–V* curves of the DSCs made with Pt, CNFs-CE on the FTO glass and ITO flexible cell, and the measurement were performed under the light intensity of 100 mW cm^{-2} (1.5 AM). To effectively use CNFs as a flexible CE in DSC, the device performance and the sintering conditions were initially optimized on the standard FTO glass based DSCs and quasi-solid state electrolyte was used. The photovoltaic parameters derived from Fig. 6 are given in Table 1. The device made with the CNFs-CE on the FTO glass exhibited 7.0% energy conversion efficiency (η), with short-circuit current density (J_{SC}) around 12.0 mA cm^{-2}, open-circuit voltage (V_{OC}) over 0.825 V, and fill factor (FF) more than 69.0%, respectively. The values are comparable to DSCs made with the Pt CE, which showed J_{SC} of 12.3 mA cm^{-2}, V_{OC} of 0.818 V, FF of 71.0%, and η of 7.1%. It is clear that the average V_{OC} of both CNFs is larger than that of the Pt cells by 0.15 V. This reflects the efficient catalytic ability of the CNF electrodes, which makes the potential of I^-/I_3^- redox reaction higher [6,10,37]. Nevertheless, the CNF based cells showed a little lower J_{SC} and FF as compared to the Pt based cells. There might be two reasons; higher total internal series resistance caused by the thick catalyst layer and the opaque nature of the blackish thick CNF layer, which cannot induce a light reflection effect [12,22,38]. In the case of the Pt CE, the island-like structure of Pt and its semitransparent nature leads to a low internal resistance with the good light reflection to yield higher J_{SC}. These trends are clearly seen in the *I–V* curve and EIS analysis. Thick CNFs or any good carbon catalyst layer may have positive effect on I_3^- reduction by having high surface area but it leads to the higher internal series resistance [11]. The presence of the thick catalyst layer increases the Nernst diffusion impedance for CNF electrodes which is much larger than the thin Pt electrodes [12,15].

Table 1
Photovoltaic parameters of the DSCs made with both FTO glass and ITO flexible counter electrodes filled with liquid electrolyte.

Counter electrode catalyst	R_{CT} ($\Omega\,cm^2$)	FTO glass/liquid electrolyte				ITO plastic/liquid electrolyte			
		J_{SC} (mA cm^{-2})	V_{OC} (V)	FF (%)	η (%)	J_{SC} (mA cm^{-2})	V_{OC} (V)	FF (%)	η (%)
Bare FTO	–	1.7	0.826	4.7	0.06	–	–	–	–
Pt	1.2	12.3	0.818	71.0	7.1	12.2	0.806	65.8	6.6
CNF-LSA	0.5	12.1	0.830	69.7	7.0	12.0	0.818	64.9	6.5
CNF-100	0.6	12.0	0.826	69.0	6.8	12.2	0.801	65.1	6.4

R_{CT}, charge transfer resistance, J_{sc}, short circuit current, V_{oc}, open circuit voltage, FF, fill factor. All values are averages of three cells and the active area of the device was 0.25 cm^2.

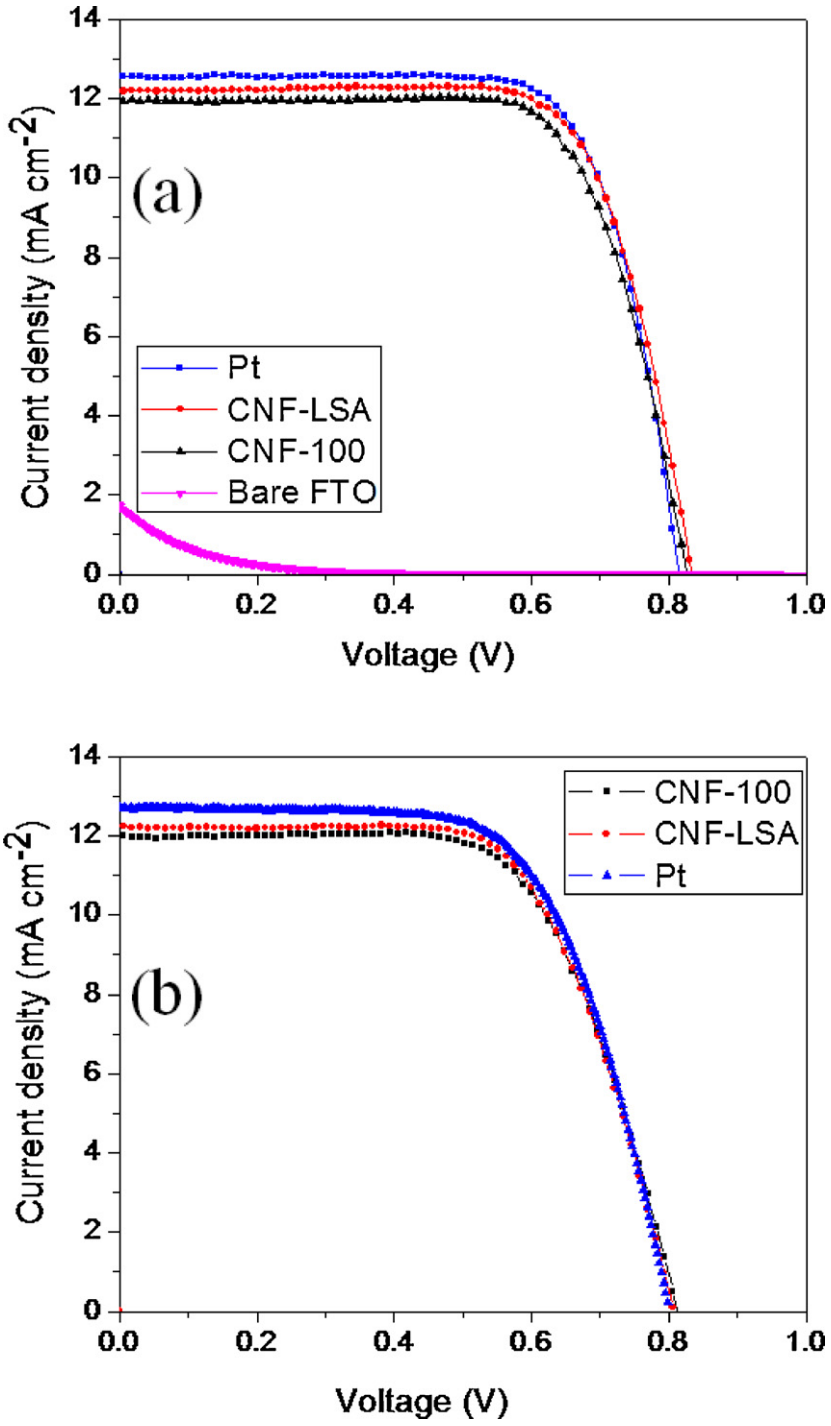

Fig. 6. Photocurrent–voltage curves for liquid electrolyte DSC with CNFs or Pt deposited on (a) FTO glass substrate and (b) on ITO/PET flexible substrate as CE.

3.3.2. CNF counter electrode on ITO/PET plastic with liquid electrolyte

The DSCs made with CNFs as a counter electrode catalyst on flexible ITO/PET with liquid electrolyte yielded an efficiency of more than 6.0%, which is almost comparable with sputtered Pt counter electrode on ITO/PET. Their respective *I–V* curves and photovoltaic parameters were shown in Fig. 6b and Table 1. The CNFs-CE on the flexible plastic substrates showed a promising performance with the volatile liquid electrolyte. The use of CNFs with a large pore diameter in the film and randomly oriented mesoporous fiber network was further demonstrated in quasi-solid state flexible CE DSCs.

3.3.3. CNF counter electrode on ITO/PET plastic with quasi-solid state electrolyte

The DSCs fabricated with the low temperature CNFs-CE on ITO/PET using the quasi-solid state electrolyte achieved high conversion efficiency (η) of 5.4% and 4.9%, (Fig. 7), respectively which is more than 85% of the device performance when compared with the Pt CE (6.0%) on ITO/PET. The device performance parameters

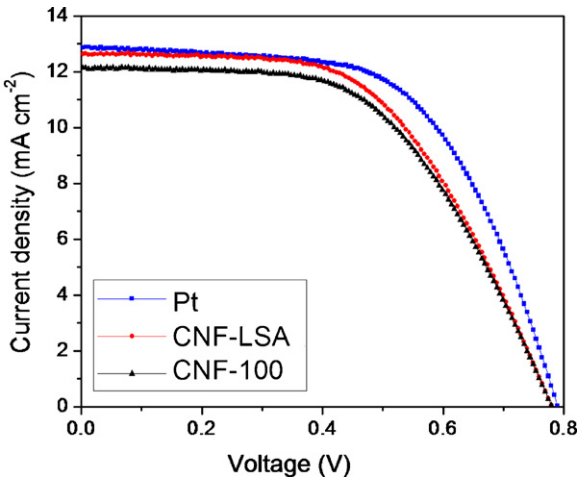

Fig. 7. Photocurrent–voltage curves for quasi-solid state electrolyte DSC with CNFs or Pt deposited on ITO/PET flexible substrate as CE.

Table 2
Photovoltaic parameters of the DSCs with flexible ITO/PET counter electrodes and quasi-solid state electrolyte.

Flexible counter electrode catalyst	Quasi electrolyte			
	J_{SC} (mA cm^{-2})	V_{OC} (V)	FF (%)	η (%)
CNF-LSA	12.6	0.779	55.2	5.4
CNF-100	12.1	0.779	52.5	4.9
Pt	12.9	0.789	59.3	6.0

J_{sc}, short circuit current, V_{oc}, open circuit voltage, FF, fill factor. All values are averages of three cells and the active area of the device was 0.25 cm^2.

are summarized in Table 2. Though photovoltaic performance in the liquid state DSCs is high, they have side effects with the electrolyte leakage problems that have hindered their widespread practical applications [9,19,20]. Both CNFs showed similar J_{SC} and V_{OC} but CNF-LSA showed superior I_3^- reduction in the quasi-solid state electrolyte. This was also confirmed with the EIS analysis (lower R_{CT}) and higher FF. Substantially better FF is achieved from the penetration of the viscous polymer-gel electrolyte in the antler structure on the walls of CNF-LSA compared with the CNF-100, which does not have completely opened structure (see Figs. 1 and 5). CNFs-CE based device performance is nearly comparable with the sputter deposited Pt on the ITO/PET flexible substrate with the quasi-solid state electrolyte (6.0%). Small difference in the power conversion efficiency for Pt and CNFs-CE might be from the higher sheet resistance and the internal series resistance originating from the thick CNFs-CE, which contributes to the low FF and J_{SC} [12,13,35]. Use of the conductive flexible ITO/PET films and stable quasi-solid electrolyte in DSCs has a huge advantage. FTO and Pt are some of the expensive components in DSCs but replacing those materials with the above mentioned low cost and stable alternative quasi-solid electrolyte decreases the cost, stability [39] and this allows the possibility of roll to roll production processes for the large scale applications.

3.3.4. *Room temperature stability of CNF and Pt counter electrode*

Stability is one of the main concerns when using alternative CE in DSCs [11]. Here, we measured the stability of our sealed cells once in 24 h for 240 h (Fig. 8). Before and after the measurement, cells were stored in dark at room temperature. The new devices are made on FTO glass based CNF and Pt-CE with liquid electrolyte as a redox mediator. In the short-term evaluation test, V_{OC} of the cell with CNF increased slightly more than Pt when compared with the freshly prepared cells. In contrast, J_{SC} started decreasing as days passed and this trend is higher in the cell with CNF-CE. All the cells were made with similar experimental conditions and sealed properly with surlyn and cover glass, thick carbon layer might have adsorbed moisture with ease, when compared with Pt [40]. But the decrease in J_{SC} has been compensated by increase in V_{OC} and the stable FF. This is resulted either from the shift in the conduction band of the TiO_2 toward negative values or the I^-/I_3^- redox energy level shift to the positive values [10,11]. Even with the small degradation in J_{SC} for CNF-CE, the device maintained 90% of initial day performance.

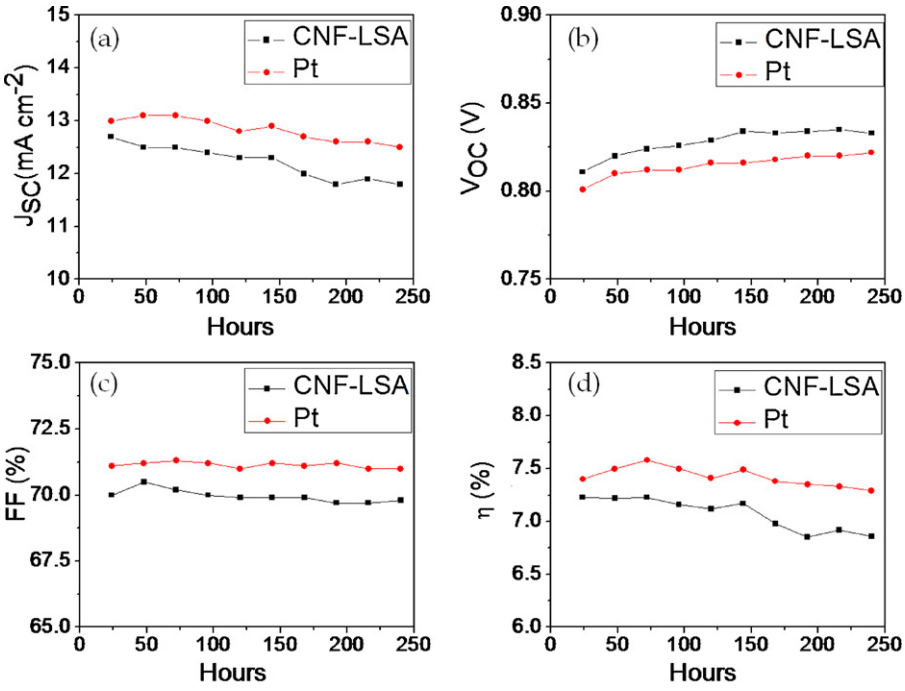

Fig. 8. Short time evaluation of *I–V* parameters in DSCs with CNF-LSA and Pt, (a) short-circuit current density, J_{SC}; (b) open-circuit voltage, V_{OC}; (c) fill-factor, FF; (d) energy conversion efficiency, η.

4. Conclusions

Carbon-nanofibers (CNFs) with unique antler and herring-bone structure were successfully used as a low temperature counter electrode catalyst for I_3^- reduction catalyst in liquid and quasi-solid state DSCs. Carbon-nanofibers have unique structural property with terminated graphitic layers in the surface of the fibers, defect rich edge planes and bigger pore diameter in film, including rough surface and large surface area. Due to these facts, CNF shows faster electron transfer kinetics with considerable improvement in photovoltaic performance. Furthermore, the use of CNFs-CE at low temperature enabled good performance flexible DSCs with stable quasi-solid state electrolyte. All the devices made with the CNFs-CE showed comparable energy conversion efficiency and good stability with the traditional Pt CE. To achieve better photovoltaic performance, thickness optimization of CNFs-CE is in progress, which may reduce the internal series resistance and diffusion impedance caused by the thick catalytic layer.

Acknowledgments

This work was supported by the Korea Research Foundation (KRF) through the National Research Laboratory Project and the nano fusion program of the POSCO. The authors would like to thank Dr. B. Karunagaran for his fruitful discussions.

References

[1] B. O'Regan, M. Grätzel, Nature 353 (1991) 737–740.
[2] M.K. Nazeeruddin, A. Kay, I. Rodicio, R. H-Baker, E. Miller, P. Liska, N. Vlachopoulos, M. Grätzel, J. Am. Chem. Soc. 115 (1993) 6382–6390.
[3] Y. Chiba, A. Islam, Y. Watanabe, R. Komiya, N. Koide, L.Y. Han, J. Appl. Phys. 45 (2006) L638–L640.
[4] S.W. Rhee, W. Kwon, Kor. J. Chem. Eng. 28 (2011) 1481–1494.
[5] N. Papageorgiou, Coord. Chem. Rev. 248 (2004) 1421–1446.
[6] A. Hauch, A. Georg, Electrochim. Acta 46 (2001) 3457–3466.
[7] R. Bashyam, P. Zelenary, Nature 443 (2006) 63–66.
[8] H. Zhu, H. Zeng, V. Subramanian, C. Masarapu, K.-H. Hung, B. Wei, Nanotechnology 19 (2008) 465204–465209.
[9] E. Ramasamy, J.W. Lee, Chem. Commun. 46 (2010) 2136–2138.
[10] K. Imoto, K. Takahashi, T. Yamaguchi, T. Komura, J. Nakamura, K. Murata, Sol. Energy Mater. Sol. Cells 79 (2003) 459–469.
[11] V. Ganapathy, B. Karunagaran, S.W. Rhee, ACS Appl. Mater. Interfaces 3 (2011) 857–862.
[12] T.N. Murakami, S. Ito, Q. Wang, Md.K. Nazeeruddin, T. Bessho, I. Cesar, P. Liska, R. H- Baker, P. Comte, P. Pechy, M. Grätzel, J. Electrochem. Soc. 153 (2006) A2255–A2261.
[13] E. Ramasamy, W.J. Lee, D.Y. Lee, J.S. Song, Appl. Phys. Lett. 90 (2007) 173103–173113.
[14] K.-C. Huang, Y.-C. Wang, R.X. Dong, W.-C. Tsai, K.-W. Tsai, C.-C. Wang, Y.-H. Chen, R. Vittal, J.-J. Lin, K.-C. Ho, J. Mater. Chem. 20 (2010) 4067–4073.
[15] G.-R. Li, F. Wang, Q.-W. Jiang, X.-P. Gao, P.-W. Shen, Angew. Chem. Int. Ed. 49 (2010) 1–5.
[16] J.D.R. Mayhew, J.D. Bozym, C. Punckt, I.A. Aksay, ACS Nano 4 (2010) 6203–6211.
[17] J.B. Xia, N. Masaki, K.J. Jiang, S. Yanagida, J. Mater. Chem. 17 (2007) 2845–2850.
[18] J. Chen, K. Li, Y. Luo, X. Guo, D. Li, M. Deng, S. Huang, Q. Meng, Carbon 47 (2009) 2704–2708.
[19] P. Wang, S.M. Zakeeruddin, J.E. Moser, M.K. Nazeeruddin, T. Sekiguchi, M. Grätzel, Nat. Mater. 2 (2003) 402–407.
[20] M.Y. Song, Y.R. Ahn, M. Jo, D.Y. Kim, J.P. Ahn, Appl. Phys. Lett. 87 (2005) 113113–113123.
[21] T. Yamaguchi, N. Tobe, D. Matsumoto, H. Arakwa, Chem. Commun. (2007) 4767–4769.
[22] M. Wang, A.M. Anghel, B. Marsan, N.C. Ha, N. Pootrakulchote, S.M. Zakeeruddin, M. Grätzel, J. Am. Chem. Soc. 131 (2009) 15976–15977.
[23] K. Aitola, A. Kaskela, J. Halme, V. Ruiz, A.G. Nasibulin, E.I. Kauppinen, P.D. Lund, J. Electrochem. Soc. 157 (2010) B1831–B1837.
[24] L.L. Chen, J. Liu, J.B. Zhang, X.W. Zhou, X.L. Zhang, Y. Lin, Chin. Chem. Lett. 21 (2010) 1137–1140.
[25] J.E. Trancik, S.C. Barton, J. Hone, Nano Lett 8 (2008) 982–987.
[26] C.E. Banks, T.J. Davies, G.G. Wildgoose, R.G. Compton, Chem. Commun 7 (2005) 829–841.
[27] C.E. Banks, A. Crossleym, C. Salter, S.J. Wilkins, R.G. Compton, Angew. Chem. Int. Ed. 45 (2006) 2533–2537.
[28] C.E. Banks, R.G. Compton, Analyst 131 (2006) 15–21.
[29] S. Shanmugam, A. Gadanken, Electrochem. Commun. 8 (2006) 1099–1105.
[30] T.-C. Wei, C.-C. Wan, Y-Y. Wang, C.-M. Chen, H.-S. Shiu, J. Phys. Chem. C 111 (2007) 4847–4853.
[31] N. Papageorgiou, W.F. Maier, M. Grätzel, J. Electrochem. Soc. 144 (1997) 876–884.
[32] J. Van de Lagemaat, N.G. Park, A.J. Frank, J. Phys. Chem. B 104 (2000) 2044–2052.
[33] F.F. Santiago, J. Bisquert, E. Palomares, L. Otero, D. Kuang, S.M. Zakeeruddin, M. Grätzel, J. Phys. Chem. C 111 (2007) 6550–6560.
[34] V. Ganapathy, B. Karungaran, S.W. Rhee, J. Power Sources 19 (2010) 5138–5143.
[35] L. Han, N. Koide, Y. Chiba, A. Islam, R. Komiya, N. Fuke, A. Fuki, R. Yamanaka, Appl. Phys. Lett. 86 (2005) 213501–213503.
[36] N. Koide, A. Islam, Y. Chiba, L. Han, J. Photochem. Photobiol. A 182 (2006) 296–305.
[37] C.-H. Zhou, Y. Yang, J. Zhang, S. Xu, S.-J. Wu, H. Hu, B.-L. Chen, Q.-D. Tai, Z.-H. Sun, X.-Z. Zhao, Electrochim. Acta 54 (2009) 5320–5325.
[38] R.R. Jia, J. Chen, J. Zhao, J. Zheng, C. Song, L. Li, Z. Zhu, J. Mater. Chem. 20 (2010) 10829–10834.
[39] J.M. Kroon, N.J. Bakker, H.J.P. Smit, P. Liska, K.R. Thambi, P. Wang, S.M. Zakeeruddin, M. Grätzel, A. Hinsch, S. Hore, U. Wurfel, R. Sastrawan, J.R. Durrant, E. Palomares, H. Pettersson, T. Gruszecki, J. Walter, K. Skupien, G.E. Tulloch, Prog. Photovoltaic: Res. Appl. 15 (2007) 1–18.
[40] M.K. Nazeeruddin, A. Kay, I. Rodicio, R.H. Baker, E. Muller, P. Liska, N. Vlachopoulos, M. Grätzel, J. Am. Chem. Soc. 115 (1993) 6382–6390.